Supplementary Information for "Individually Addressed Entangling Gates in a Two-Dimensional Ion Crystal"

Y.-H. Hou,[1,*] Y.-J. Yi,[1,*] Y.-K. Wu,[1,2,*] Y.-Y. Chen,[1] L. Zhang,[1] Y. Wang,[1,3] Y.-L. Xu,[1] C. Zhang,[1,3] Q.-X. Mei,[3] H.-X. Yang,[3] J.-Y. Ma,[3] S.-A. Guo,[1] J. Ye,[1] B.-X. Qi,[1] Z.-C. Zhou,[1,2] P.-Y. Hou,[1,2] and L.-M. Duan[1,2,4,†]

[1] *Center for Quantum Information, Institute for Interdisciplinary Information Sciences, Tsinghua University, Beijing 100084, PR China*
[2] *Hefei National Laboratory, Hefei 230088, PR China*
[3] *HYQ Co., Ltd., Beijing 100176, PR China*
[4] *New Cornerstone Science Laboratory, Beijing 100084, PR China*

Supplementary Note 1 — Alternating two-qubit gates in large ion crystals

In the main text, we use phase-modulated pulse sequences to disentangle the spin and the phonon modes exactly. However, its required segment number increases exponentially with the number of phonon modes to be decoupled [1], which is inefficient for large ion crystals. Fortunately, previous works already show that we can use a much smaller number of segments to disentangle the spin and the phonon modes approximately, while still achieving high gate fidelities (see, e.g. Refs. [2, 3]). In principle we can use any degrees of freedom like the amplitude, phase or frequency of the laser to optimize the gate performance. In practice, finding an amplitude-modulated gate sequence is often easier: The direct optimization of gate infidelity can be formulated as a generalized eigenvalue problem, and even with the robustness criteria included, it can still be expressed as an optimization of polynomial functions [4]. Therefore, here we present results for an alternating gate sequence on two target ions with amplitude modulation.

Following the derivation of Ref. [4], we divide the total gate time into n_{seg} equal segments with piecewise-constant Raman Rabi rate given by a real vector $\mathbf{\Omega} = (\Omega_1, \Omega_2, \cdots, \Omega_{n_{\text{seg}}})^T$. The optimization of the spin-dependent displacement [Eq. (1) of the main text] and the two-qubit phase [Eq. (2) of the main text], as well as their robustness against small drifts in the trap frequency, can then be expressed as a quartic function of $\mathbf{\Omega}$ (see Appendix B of Ref. [4])

$$\Omega^T \mathbf{M} \Omega + (\Omega^T \gamma \Omega)^2, \tag{1}$$

where the matrix elements of $\mathbf{M}$ and γ come from the time integral in Eqs. (1) and (2) of the main text on the corresponding segments under unit Rabi rate.

Now for an alternating pulse sequence, we can still write it as a single vector $\mathbf{\Omega} = (\Omega_1, \Omega_2, \cdots, \Omega_{n_{\text{seg}}})^T$, knowing that this sequence is to be alternatingly applied on the two target ions. To ensure this in the formulation of the optimization problem, we simply set the spin-dependent displacement on the corresponding segments and the two-qubit phase on the corresponding segment pairs to zero, which gives us a modified matrix $\mathbf{M}$ and a modified matrix γ. We optimize this cost function under the constraint that the accumulated two-qubit phase, which is quadratic in $\mathbf{\Omega}$, is equal to $\pm\pi/4$.

We present some numerical results in Supplementary Figure 1 for a 2D ion crystal of $N = 100$ ions in a harmonic trap with $\omega_x = 2\pi \times 0.7\,\text{MHz}$, $\omega_y = 2\pi \times 3\,\text{MHz}$ and $\omega_z = 2\pi \times 0.2\,\text{MHz}$. An actual 2D crystal will be subjected to micromotion, but as shown in Ref. [5], for even larger crystals, the micromotion amplitude can still be much smaller than the ion spacings such that individual addressing can still be achieved with low crosstalk. Then as we show in the main text, the effect of the micromotion can be compensated by a recalibration of the laser intensity.

We consider two target ions colored in red and blue in Supplementary Figure 1**a**. We fix a total gate time of $300\,\mu\text{s}$ and a segment number of $n_{\text{seg}} = 240$. Note that here we apply the same amplitude modulation sequence to the two target ions alternatingly and require a time reversal symmetry in the sequence (see Supplementary Figure 1**c**). Therefore, in the $n_{\text{seg}} = 240$ segments there are only $n_{\text{seg}}/4 = 60$ adjustable parameters, smaller than the number of phonon modes to be distentangled exactly. As shown in Refs. [3, 6], utilizing the locality in the spatial or the frequency domain, many distant ions or phonon modes can be neglected, allowing efficient gate design for even larger ion crystals. We further scan the Raman laser detuning and optimize the gate fidelity as the red curve in Supplementary Figure 1**b**. We obtain the gate sequence in Supplementary Figure 1**c** at the detuning $\mu = 2\pi \times 3.0194\,\text{MHz}$, namely $2\pi \times 19.4\,\text{kHz}$ above the COM mode, with a theoretical gate fidelity above 99.99% assuming an average phonon number of 0.5 for

* These authors contribute equally to this work
† lmduan@tsinghua.edu.cn

each mode. As a comparison, we also present a gate design when the laser beams are applied on the two target ions simultaneously. For a fair comparison, we use $n_{\rm seg} = 120$ segments so that there are again 60 adjustable parameters when we require the amplitude modulation sequence to be time-reversible. We set a duration of $1.25\,\mu$s for each segment and wait for another $1.25\,\mu$s between adjacent segments so that the total gate time is still $300\,\mu$s. The result is shown as the blue curve in Supplementary Figure 1**b**. As we can see, the two curves have similar tendency, which suggests that using alternating gate sequence does not harm the gate performance.

Finally, note that we may not need to achieve all-to-all coupling for all the ions. (For more distant ion pairs, this may be achieved at the cost of longer gate time and more complicated pulse sequences.) Just achieving direct two-qubit entangling gates for ion pairs within a constant distance, say, 5 to 10 ion spacings, already supports universal quantum computation while largely reducing the overhead for compiling the quantum circuit compared with the nearest-neighbor connectivity.

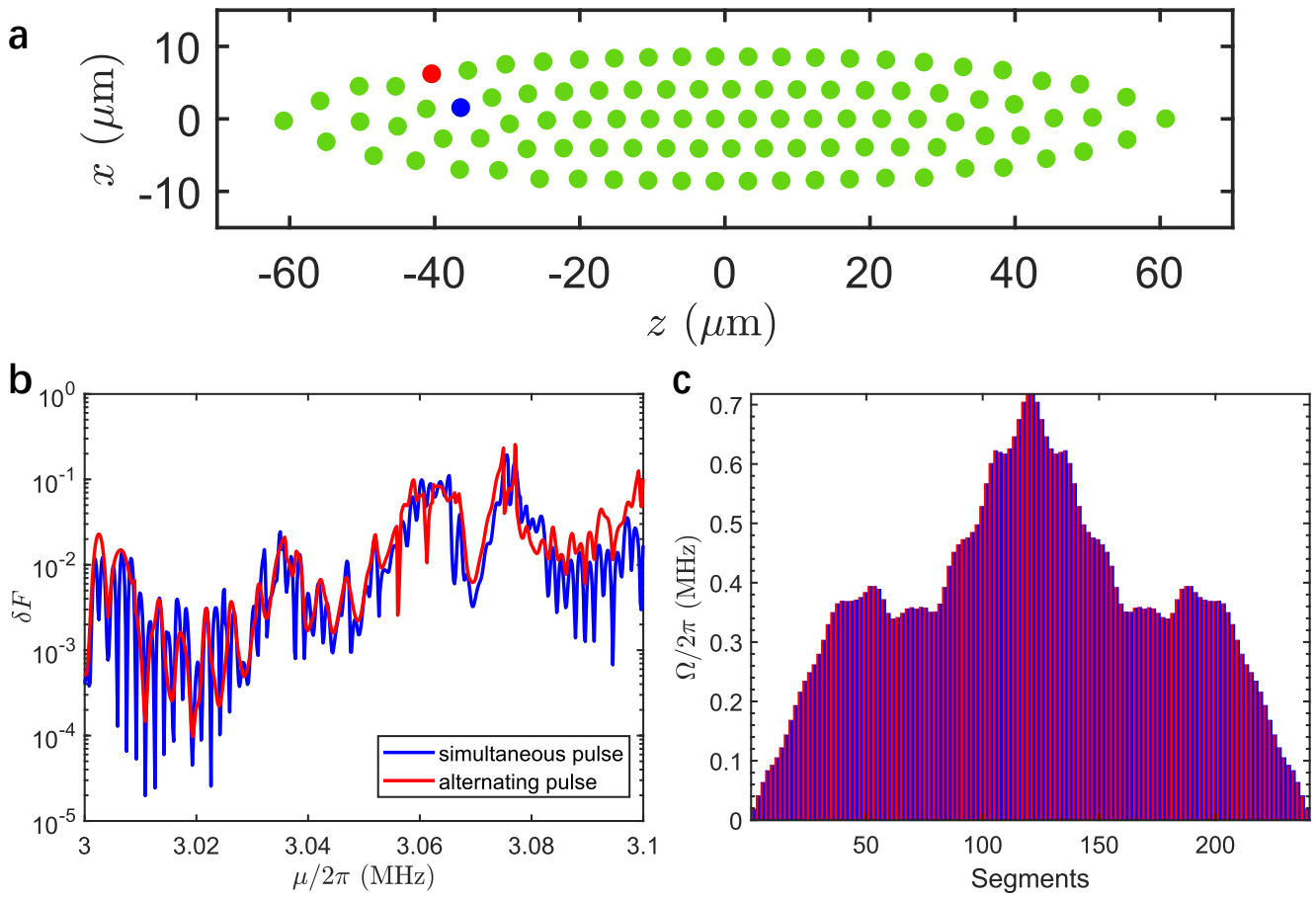

Supplementary Figure 1. **a**, A 2D ion crystal of $N = 100$ ions in a harmonic trap with $\omega_x = 2\pi \times 0.7\,$MHz, $\omega_y = 2\pi \times 3\,$MHz and $\omega_z = 2\pi \times 0.2\,$MHz. Two target ions are colored in red and blue, respectively. **b**, Optimized gate infidelity for the amplitude-modulated simultaneous-pulse gate (blue) and the alternating-pulse gate (red) vs. the laser detuning μ. We fix a gate time of $300\,\mu$s and use $n_{\rm seg} = 120$ symmetric segments for the simultaneous-pulse gate and $n_{\rm seg} = 240$ symmetric segments for the alternating-pulse gate. **c**, Optimized alternating gate sequence at the detuning $\mu = 2\pi \times 3.0194\,$MHz, namely $2\pi \times 19.4\,$kHz above the COM mode. The red and blue colors correspond to the laser sequences that are alternatingly applied on the two target ions, respectively. The theoretical gate infidelity is below 10^{-4}.

Supplementary Note 2 — Scalability of 2D addressing system

To apply our 2D addressing scheme to larger ion crystals, it is necessary to consider many technical factors like the number of resolvable spots of the AODs and the optical access of the imaging system. The number of resolvable

spots is given by [7]

$$N = \frac{\Delta f \cdot D}{v} \tag{2}$$

where Δf is the bandwidth of the AOD, D the aperture, and v the acoustic velocity. For the AODs we use in this experiment (ISOMET, D1384-aQ170-7), about 100 resolvable spots can be obtained with a switching time $\tau = D/v$ of about one microsecond. Suppose we separate the ions by at least twice the diffraction limit for the crosstalk of the Raman beams to be below 10^{-4}, the number of ions that can be addressed along each direction can be estimated to be $N/2 = 50$. Allowing slower switching speed, the number of resolvable spots can be further increased. Also note that the individual addressing of above 50 ions by an AOD has already been demonstrated in the experiment [8].

The above analysis suggests that a 2D array with about $50^2 = 2500$ sites can be addressed by the crossed AODs. The required deflection angle of the laser is also given by $50/2 = 25$ ions from the center in each direction, thus within the available optical access of the current trap design. However, as we describe in the main text, for a 2D ion crystal in a Paul trap, another restriction to the addressing system comes from the micromotion of the ions. To avoid the crosstalk when controlling adjacent ions, we may want the micromotion amplitudes to be smaller than the ion spacing. Therefore, to maximize the available qubit number, we may arrange the trap potential to hold the 2D crystal in the shape of an ellipse with its major axis aligned in the axial direction without micromotion. An example with 512 ions has been demonstrated in Ref. [5]. For a trap with a Mathieu parameter $q = 0.13$ and a typical ion spacing of about $d = 5\,\mu$m on the edge, we thus limit the length of the minor axis to be at most $r = 15d$ for the micromotion amplitude $A = qr/2$ to be smaller than d. A rough estimation of the available ion number can be given by $2 \times 15 = 30$ rows, each with 50 ions, thus totally $30 \times 50 = 1500$. Another way is to assume a triangular lattice and to count the number of elementary triangles in the total area of the ellipse. Note that each elementary triangle contains $3/6 = 1/2$ ions on average. This gives us an estimation of $\pi \times 25 \times 15/(\sqrt{3}/4) \times 1/2 = 1360$ ions.

Supplementary Note 3 — Supplementary figures

The blade trap design for 2D ion crystals as mentioned in Methods is sketched in Supplementary Figure 2.

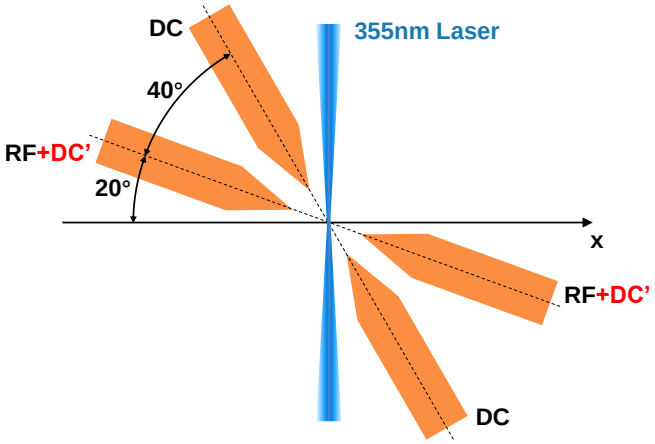

Supplementary Figure 2. Side view of our blade trap for 2D ion crystals. A DC bias (DC′) is applied on the RF electrodes to split the radial trap frequencies. The 2D ion crystal locates close to the xz plane, perpendicular to the counter-propagating 355 nm Raman laser beams and the imaging system in the y direction.

Additional data for individual addressing of different target ions in the four-ion crystal are shown in Supplementary Figure 3, similar to Fig. 1**c** and **d** of the main text.

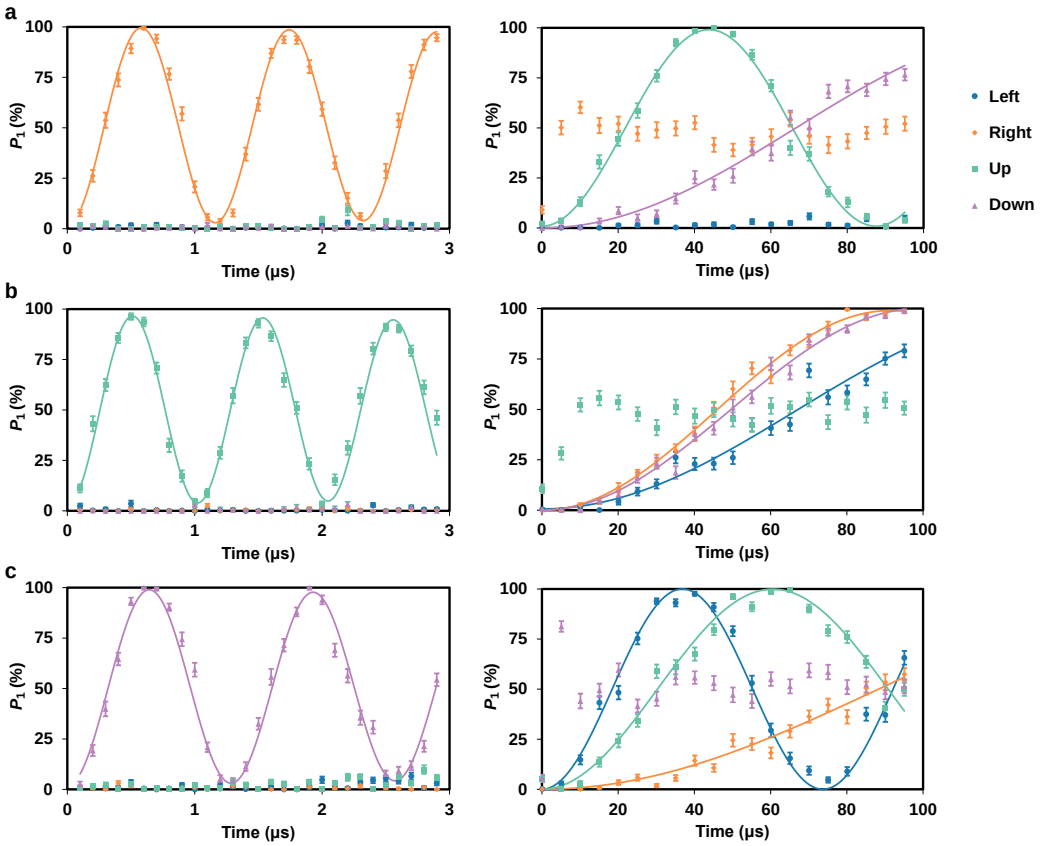

Supplementary Figure 3. Individual addressing of **a**, the right ion, **b**, the up ion, and **c**, the down ion. The left and the right panels show the short-time and the long-time Rabi oscillations, respectively. Due to the aberration of the addressing beams, the crosstalk errors are not exactly symmetric, but for all the target ions we can bound the crosstalk infidelity for a single-qubit π pulse to be below 0.08%. All the error bars represent one standard deviation.

[1] Todd J. Green and Michael J. Biercuk, "Phase-Modulated Decoupling and Error Suppression in Qubit-Oscillator Systems," Physical Review Letters **114**, 120502 (2015).

[2] Shi-Liang Zhu, C. Monroe, and L.-M. Duan, "Arbitrary-speed quantum gates within large ion crystals through minimum control of laser beams," Europhys. Lett. **73**, 485–491 (2006).

[3] K. A. Landsman, Y. Wu, P. H. Leung, D. Zhu, N. M. Linke, K. R. Brown, L. Duan, and C. Monroe, "Two-qubit entangling gates within arbitrarily long chains of trapped ions," Phys. Rev. A **100**, 022332 (2019).

[4] Y.-K. Wu, Z.-D. Liu, W.-D. Zhao, and L.-M. Duan, "High-fidelity entangling gates in a three-dimensional ion crystal under micromotion," Phys. Rev. A **103**, 022419 (2021).

[5] S.-A. Guo, Y.-K. Wu, J. Ye, L. Zhang, W.-Q. Lian, R. Yao, Y. Wang, R.-Y. Yan, Y.-J. Yi, Y.-L. Xu, B.-W. Li, Y.-H. Hou, Y.-Z. Xu, W.-X. Guo, C. Zhang, B.-X. Qi, Z.-C. Zhou, L. He, and L.-M. Duan, "A site-resolved two-dimensional quantum simulator with hundreds of trapped ions," Nature **630**, 613–618 (2024).

[6] G.-D. Lin, S.-L. Zhu, R. Islam, K. Kim, M.-S. Chang, S. Korenblit, C. Monroe, and L.-M. Duan, "Large-scale quantum computation in an anharmonic linear ion trap," Europhysics Letters **86**, 60004 (2009).

[7] Jr. Eddie H. Young and Shi-Kay Yao, "Design considerations for acousto-optic devices," Proceedings of the IEEE **69**, 54–64 (1981).

[8] M. K. Joshi, F. Kranzl, A. Schuckert, I. Lovas, C. Maier, R. Blatt, M. Knap, and C. F. Roos, "Observing emergent hydrodynamics in a long-range quantum magnet," Science **376**, 720–724 (2022).